Nearest-neighbor distributions and tunneling splittings in interacting many-body two-level boson systems

Saúl Hernández-Quiroz*
Instituto de Ciencias Físicas, Universidad Nacional Autónoma de México (UNAM), 62210 Cuernavaca, Morelos, Mexico and Facultad de Ciencias, Universidad Autónoma del Estado de Morelos (UAEM), 62209 Cuernavaca, Morelos, Mexico

Luis Benet†
Instituto de Ciencias Físicas, Universidad Nacional Autónoma de México (UNAM), 62210 Cuernavaca, Morelos, Mexico
(Received 19 November 2009; published 24 March 2010)

We study the nearest-neighbor distributions of the k-body embedded ensembles of random matrices for n bosons distributed over two-degenerate single-particle states. This ensemble, as a function of k, displays a transition from harmonic-oscillator behavior ($k=1$) to random-matrix-type behavior ($k=n$). We show that a large and robust quasidegeneracy is present for a wide interval of values of k when the ensemble is time-reversal invariant. These quasidegenerate levels are Shnirelman doublets which appear due to the integrability and time-reversal invariance of the underlying classical systems. We present results related to the frequency in the spectrum of these degenerate levels in terms of k and discuss the statistical properties of the splittings of these doublets.

DOI: 10.1103/PhysRevE.81.036218 PACS number(s): 05.45.Mt, 05.30.Jp, 03.65.Sq, 03.65.Ge

I. INTRODUCTION

The theoretical and experimental understanding of interacting many-body quantum systems has undergone considerable development in recent years. First, random matrix theory (RMT) has been quite successful in describing the statistical properties of the fluctuations of the spectra of complex quantum systems, which include many-body interacting systems. Examples range from nuclear physics to disordered systems, including elastomechanical vibrations and quantum analog systems to classical chaotic billiards (see [1] for a detailed review). While this modeling has been quite successful, RMT is not a realistic theory since it assumes many-body forces between the constituents. More realistic stochastic model considering k body interactions are the embedded ensembles, initially introduced by Mon and French [2]. This model can be defined for fermions and bosons [3] and may be viewed as the generic models for stochasticity in many-body systems.

Second, ultracold bosonic gases confined in optical lattices have become quite important due to the relatively simplicity to handle these systems experimentally [4]. In particular, Bose-Einstein condensates (BECs) in a double-well potential is a common object of study [5]. This system exhibits a great variety of interesting quantum phenomena, such as interference [6], tunneling and self-trapping [7,8], Josephson oscillations [9], and entanglement [10].

From the theoretical point of view, the two-level bosonic systems have been addressed using the mean-field treatment of the Gross-Pitaevski equation [7,11] and the two-site Bose-Hubbard Hamiltonian. The latter can be written as [12,13]

$$H_{\mathrm{BH}} = \delta(n_1 - n_2) - J(\hat{b}_1^\dagger \hat{b}_2 + \hat{b}_2^\dagger \hat{b}_1) + \frac{U}{2}[n_1(n_1-1) + n_2(n_2-1)]. \quad (1)$$

Here, $\hat{b}_i^\dagger$ and $\hat{b}_i$ are creation and annihilation operators for a boson on the ith site ($i=1,2$) and $n_i=\hat{b}_i^\dagger \hat{b}_i$ is the total number of bosons on that level, δ is the energy difference of one-boson energies among the two sites, U is the on-site two-body interaction strength, and J is the hoping or tunneling parameter. The two-mode approximation in Eq. (1) is valid as long as the interaction energy U is much smaller than the level spacing of the external trap [7].

The experimental observation of macroscopic tunneling of bosons in a double well when the initial difference of population is below a critical value [8], predicted in Ref. [7], can be understood from the spectral properties of Eq. (1). For the simpler case $\delta=0$, the spectrum consists of a lower region of nearly equidistant levels and an upper one displaying nearly degenerate doublets. The latter are actually responsible for the suppression of tunneling; it has also been shown that coherences among nearby doublets yield oscillations with very small amplitude [14]. Taking the semiclassical limit, the system has a phase-space representation similar to a pendulum, with the almost equidistant levels being associated with the libration zone and the nearly degenerate levels with the rotation zones.

In this paper, we study the statistical properties of the spectrum of n bosons distributed on two levels coupled through random k-body interactions. Thus, we merge the successful stochastic modeling of RMT with systems of the form of Eq. (1). This ensemble is actually a generalization of the Bose-Hubbard type of Hamiltonians, in particular with respect to the range of the interaction k. Each member of the ensemble is Liouville integrable (independently of k) in the classical limit [15]. Yet, the spectral statistics of the ensemble correspond to a picket fence for $k=1$ and follow

*saul@cicc.unam.mx
†benet@fis.unam.mx

RMT predictions for $k=n$ [16]. These facts make the ensemble somewhat special: completely integrable systems are associated with Poisson statistics, which is known as the Berry-Tabor conjecture [17]. In addition, the spectral fluctuations of classically fully chaotic systems typically follow RMT predictions, which is known as the Bohigas-Giannoni-Schmit (or quantum-chaos) conjecture [18]. We shall thus study the transition in the spectral statistics in terms of k, considering the nearest-neighbor distribution as well as the occurrence and statistics of tunneling splittings. We shall address this for the case when the ensemble is time-reversal invariant ($\beta=1$) or when this symmetry is broken ($\beta=2$). We find a systematic appearance of quasidegeneracies on a large interval of k for the time-reversal case, which points out the underlying integrability properties of the members of the ensemble due to a theorem by Shnirelman [19,20]. Moreover, the number of such doublets as well as the statistics of the associated splittings display a dependence upon k. These results may be interesting for the understanding and modeling of three-body interactions in cold gases [21].

The paper is organized as follows. In Sec. II, we present the k-body embedded ensembles of random matrices for two-level boson systems and review some important properties of this ensemble. In Sec. III, we discuss the nearest-neighbor distribution of the ensembles in terms of the interaction parameter k for both cases of Dyson's parameter β. We obtain the systematic appearance of quasidegenerate states in the spectrum linked to the $\beta=1$ case and address the dependence of their number with respect to k. In Sec. IV, we present the semiclassical limit of this ensemble and describe the structure of the corresponding phase space. Section V is devoted to the identification of the $\beta=1$ quasidegenerate states and present results on the statistical properties of their spacings. In Sec. VI, we present a summary of our results and the conclusions.

II. k-BODY INTERACTING TWO-LEVEL BOSON ENSEMBLE

We begin defining the most general k-body interaction of n spinless bosons distributed in two single-particle levels which, for simplicity, are assumed to be degenerate [case $\delta=0$ in Eq. (1)]. The single-particle states are associated with the operators $\hat{b}_j^\dagger$ and $\hat{b}_j$, with $j=1,2$, which, respectively, create or annihilate one boson on the single-particle level j. These operators satisfy the usual commutation relations for bosons. The normalized n-boson states are specified by $|\mu_r^{(n)}\rangle=(\mathcal{N}_r^{(n)})^{-1}(\hat{b}_1^\dagger)^r(\hat{b}_2^\dagger)^{n-r}|0\rangle$, where $\mathcal{N}_r^{(n)}=[r!(n-r)!]^{1/2}$ is a normalization constant and $|0\rangle$ is the vacuum state. The Hilbert-space dimension is $N=n+1$. In second-quantized form, the most general Hamiltonian $\hat{H}_k^{(\beta)}$ with k-body interactions can be written as [22]

$$\hat{H}_k^{(\beta)}=\sum_{r,s=0}^{k} v_{r,s}^{(\beta)}\frac{(\hat{b}_1^\dagger)^r(\hat{b}_2^\dagger)^{k-r}(\hat{b}_1)^s(\hat{b}_2)^{k-s}}{\mathcal{N}_r^{(k)}\mathcal{N}_s^{(k)}}. \tag{2}$$

Physically, $\hat{H}_k^{(\beta)}$ in Eq. (2) corresponds to n bosons confined, e.g., in a double-well potential, coupled only through k-body interactions. Clearly, the degenerate Bose-Hubbard model Eq. (1) is a particular choice of the parameters for the combination $\hat{H}_{k=1}^{(1)}+\hat{H}_{k=2}^{(1)}$.

Stochasticity is built into the Hamiltonian $\hat{H}_k^{(\beta)}$ at the level of the k-body matrix elements $v_{r,s}^{(\beta)}$. These matrix elements are assumed to be Gaussian-distributed independent random variables with zero mean and constant variance $v_0^2=1$. Then, $\overline{v_{r,s}^{(\beta)}v_{r',s'}^{(\beta)}}=v_0^2(\delta_{r',s}\delta_{r,s'}+\delta_{\beta,1}\delta_{r,r'}\delta_{s,s'})$, where the over line denotes ensemble average. As in the case of the canonical random matrix ensembles [1], Dyson's parameter β distinguishes the symmetry properties with respect to time-reversal invariance: $\beta=1$ corresponds to the case where time-reversal symmetry holds while the broken time-reversal case is denoted by $\beta=2$. The k-body interaction matrix $v^{(\beta)}$ is thus a member of the Gaussian orthogonal ensemble (GOE) for $\beta=1$ or Gaussian unitary ensemble (GUE) for $\beta=2$. This defines completely the k-body embedded ensemble of random matrices for bosons distributed in $l=2$ levels. Without loss of generality, in the following, we set $v_0=1$. The combinatorial factors $\mathcal{N}_r^{(k)}$ in Eq. (2) are actually introduced in order to have *an exact identity* of the embedded ensembles with the canonical ensembles of RMT when $k=n$ [3,22]. Indeed, the factors $\mathcal{N}_r^{(k)}$ cancel the square-root factors that appear by operating the $k=n$ creation and annihilation operators onto the many-body states $|\mu_r^{(n)}\rangle$. Then, the central-limit theorem implies that the matrix elements become independent Gaussian-distributed random variables; this is precisely the definition of the canonical ensembles of RMT. Consequently, for $k=n$, all spectral fluctuations correspond exactly to the predictions of RMT.

By construction, the number operator $\hat{n}=\hat{b}_1^\dagger\hat{b}_1+\hat{b}_2^\dagger\hat{b}_2$ commutes with the Hamiltonian $\hat{H}_k^{(\beta)}$ for all values of the rank of the interaction k. The Hamiltonian is thus block diagonal in the occupation-number basis $|\mu^{(n)}\rangle$ defined above. For a given value k, the number of independent random variables of the ensemble is $K_\beta(k)=\beta(k+1)(k+1+\delta_{\beta,1})/2$, which in general is smaller than the Hilbert-space dimension $N=n+1$. Therefore, for $k\ll n$, the matrix elements of the Hamiltonian $\hat{H}_k^{(\beta)}$ are correlated, i.e., the number of independent matrix elements of the Hamiltonian is larger than the number of independent random variables. Moreover, some matrix elements are identically zero.

III. SPECTRAL STATISTICS IN TERMS OF k

The evaluation of statistical measures of the spectrum requires unfolding the spectra, which removes the nonuniversal system-dependent contributions. This can be done by performing the unfolding individually for each spectrum (spectral unfolding) or by a single transformation used for all members of the ensemble (ensemble unfolding). In the context of spectral fluctuations, ergodicity implies that the results are independent of the unfolding method.

In Ref. [22], it was shown that the k-body embedded ensemble of random matrices for bosons is nonergodic in the dense limit. The dense limit is defined as the limit $n\to\infty$ with k and the number of single-particle levels l fixed. This result was obtained analytically by considering the fluctua-

tions of the centroids and variances of individual spectra, which do not vanish in the limit $n \to \infty$ of infinite Hilbert-space dimension [22]. Therefore, in the dense limit, ensemble average and spectral average yield in general different results. The nonergodic character of the ensemble in the dense limit is a consequence of the fact that each member of the ensemble is Liouville integrable in the classical limit [15]. In this case, spectral unfolding is the only physically meaningful rectification of the spectra. In the numerical results described below, we implemented it by fitting the staircase function of each member of the ensemble separately with a polynomial of maximum degree 8.

In Fig. 1, we present the nearest-neighbor spacing distribution $P_k(s)$ for various values of k, for $\beta=1$ and $n=2000$. These results were obtained after averaging over 1000 realizations of the ensemble. More details can be observed in the accompanying movie [23]. In these figures, we have included for comparison the Poisson distribution and the Wigner surmise for the GOE [1].

For $k=1$, the system corresponds to two coupled harmonic oscillators. Consequently, after unfolding, we obtain the expected distribution for an equidistant spectrum, i.e., $P_{k=1}(s)=\delta(s-1)$ [Fig. 1(a)]. As seen in Fig. 1(b), for $k=2$, this distribution changes considerably. It displays a quite large peak at $s=0$, a tail that decays somewhat slower than the Gaussian tail for larger values of s, and a broad peak around $s=1$ reminiscent of the Dirac delta obtained for $k=1$. The peak at $s=0$ indicates the occurrence of quasidegenerate energy levels and, as we shall demonstrate below, it is a consequence of the time-reversal symmetry ($\beta=1$) of the ensemble. Increasing slowly the value of k enhances the level clustering at $s=0$ and diminishes, shifts, and smoothes the peak at $s=1$. This is illustrated for $k=10$ in Fig. 1(c), where we also note that the tail of the distribution approaches the exponential decay characteristic of the Poisson distribution. The local maximum observed at $s \approx 1$ disappears smoothly by increasing the value of k, being unnoticeable already for $k=75$ [23].

By increasing the value of k, the distribution $P_k(s)$ evolves smoothly still displaying a strong degree of degeneracy at $s=0$ [cf. Figs. 1(d) and 1(e) for $k=200$ and $k=1000$, respectively]. Eventually, around $k=1150$, a new local maximum of the distribution is noticeable around $s \approx 0.3$ [Fig. 1(f)], which moves toward larger values of s for larger values of k; this peak will become the single maximum of the GOE reached at $k=n$. From here on, except for the peak at $s=0$, the distribution evolves toward the GOE results by increasing the value of k (see [23]), similarly to the transition observed in the spectral properties of the system when the dynamics of its classical analog evolves from near integrable to fully chaotic. Interestingly, the peak at $s=0$ is still observed for rather large values of k. Around $k=1850$ [Fig. 1(g)], this peak disappears, i.e., level repulsion completely sets in. Beyond $k=1900$, the distribution corresponds essentially to that of a GOE. We note that there is no value of k where $P_k(s)$ fully coincides with the Poisson distribution, although it does so for larger spacings (tail of the distribution) in an extended range of values of k. It is not clear to us how to explain such an exponential tail for intermediate values of k. At the moment, we believe that this fact may be related with a partial applicability of the original Berry-Tabor argument, which somehow cannot be extended to all tori (see Ref. [24] for some recent results discussing the generic aspects of the Berry-Tabor conjecture).

The remarkable property of the nearest-neighbor distributions described above is the appearance and robustness of the large peak found around $s=0$. This peak is not only pointing out the lack of level repulsion, but actually indicating that a relevant part of the spectrum is degenerate or quasidegenerate. This peak corresponds to the prediction of Shnirelman's theorem [19], which essentially states that smooth-enough time-reversal invariant ($\beta=1$) and integrable Hamiltonian of two degrees of freedom have an asymptotically multiple spectrum, i.e., quasidegenerate levels (see also [20]). Note that the assumptions of this theorem are fulfilled, since each member of the ensemble is Liouville integrable in the semiclassical limit [15].

To completely prove that the peak is indeed Shnirelman's peak, it suffices to consider the nearest-neighbor distribution $P_k(s)$ for an ensemble of Hamiltonians $\hat{H}_k^{(\beta)}$ with broken time-reversal invariance, i.e., $\beta=2$. If time reversal is important, the peak should disappear for $\beta=2$. The results are illustrated in Fig. 2 for different values of k, considering $n=1000$ bosons and 1000 realizations of the ensemble (see the corresponding movie [23] for more details). The figures show the transition from a picket fence spectrum ($k=1$) to a GUE ($k=n$). In particular, they show the absence of the strong peak at $s=0$ (Shnirelman's peak), even though as a function of k there is certain degree of level clustering, which are not quasidegeneracies of the type discussed above. This is further illustrated in Fig. 3, where we show the relative number of levels μ_k corresponding to the first four bins of $P_k(s)$ as a function of k, both for $\beta=1$ and $\beta=2$. In this figure, we have also included the average number of degenerate levels, which were identified using symmetric or antisymmetric combinations of the corresponding eigenfunctions (cf. Sec. V A). Figure 3 implies that, as a function of k, there are different statistical properties of the degenerate levels. This in turn suggests the use of the quasidegenerate levels, i.e., the tunneling splittings, as a possible measure to test k-body interactions in such integrable systems.

IV. SEMICLASSICAL LIMIT AND THE CLASSICAL PHASE SPACE

A. Semiclassical limit

Following Refs. [16,25], we write an appropriate semiclassical limit for the algebraic Hamiltonian $\hat{H}_k^{(\beta)}$, which will allow us to identify systematically time-reversal related symmetric or antisymmetric combinations of eigenfunctions. To this end, we symmetrize first $\hat{H}_k^{(\beta)}$ with respect to the ordering of the creation and annihilation operators by exploiting the commutation relations among the bosonic creation and annihilation operators, typically in the form $\hat{b}_r^\dagger \hat{b}_s = (\hat{b}_r^\dagger \hat{b}_s + \hat{b}_s \hat{b}_r^\dagger - \delta_{r,s})/2 (r,s=1,2)$. Then, we use Heisenberg's semiclassical rules [26]

$$\hat{b}_r^\dagger \to I_r^{1/2} \exp(i\phi_r), \quad \hat{b}_r \to I_r^{1/2} \exp(-i\phi_r), \tag{3}$$

where ϕ_r is an angle and I_r is its canonically conjugated momentum. We emphasize the fact that considering the two-

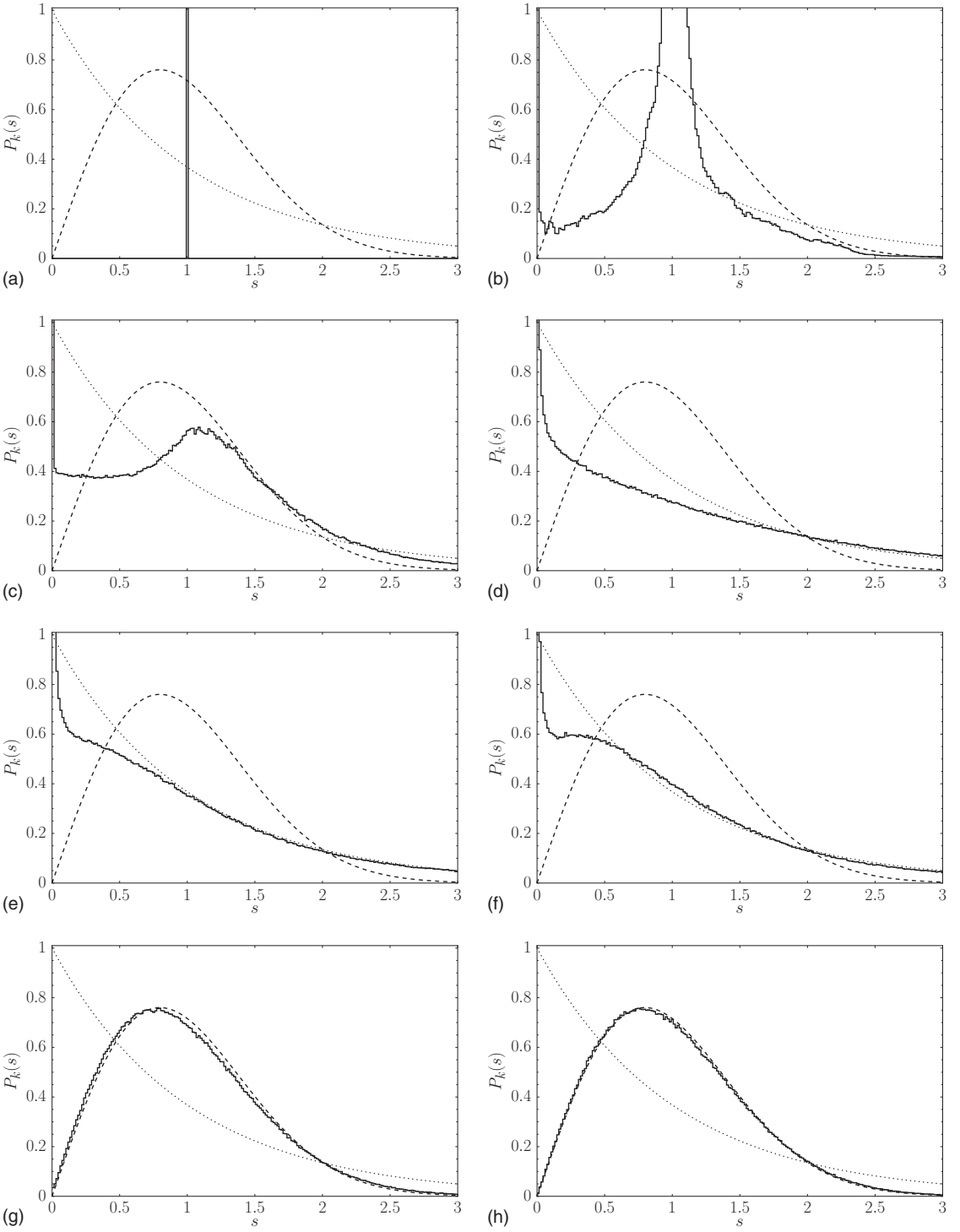

FIG. 1. Nearest-neighbor distribution $P_k(s)$ for the k-body interacting two-level boson ensemble for $\beta=1$, $n=2000$, and (a) $k=1$, (b) $k=2$, (c) $k=10$, (d) $k=200$, (e) $k=1000$, (f) $k=1150$, (g) $k=1850$, and (h) $k=2000$. Notice the large peak observed at $s=0$, which is linked with the occurrence of quasidegenerate levels. The dashed curve corresponds to the Wigner surmise for $\beta=1$, while the dotted curve is the Poisson distribution.

level case ($l=2$) implies that the classical associated Hamiltonian has two degrees of freedom.

The classical Hamiltonian obtained in this way can be written as $\mathcal{H}_k^{(\beta)}(I_1,I_2,\phi_1,\phi_2)=\mathcal{H}_{0k}^{(\beta)}(I_1,I_2)+\mathcal{V}_k^{(\beta)}(I_1,I_2,\phi_1,\phi_2)$. Here, $\mathcal{H}_{0k}^{(\beta)}(I_1,I_2)$ is a Hamiltonian that depends on the action variables only and is therefore integrable and the perturbing term $\mathcal{V}_k^{(\beta)}(I_1,I_2,\phi_1,\phi_2)$ carries all the dependence upon the angles. The first term is associated with all the diagonal contributions of $\hat{H}_k^{(\beta)}$, while the second one corresponds to all off-diagonal contributions. These terms are explicitly given by [16]

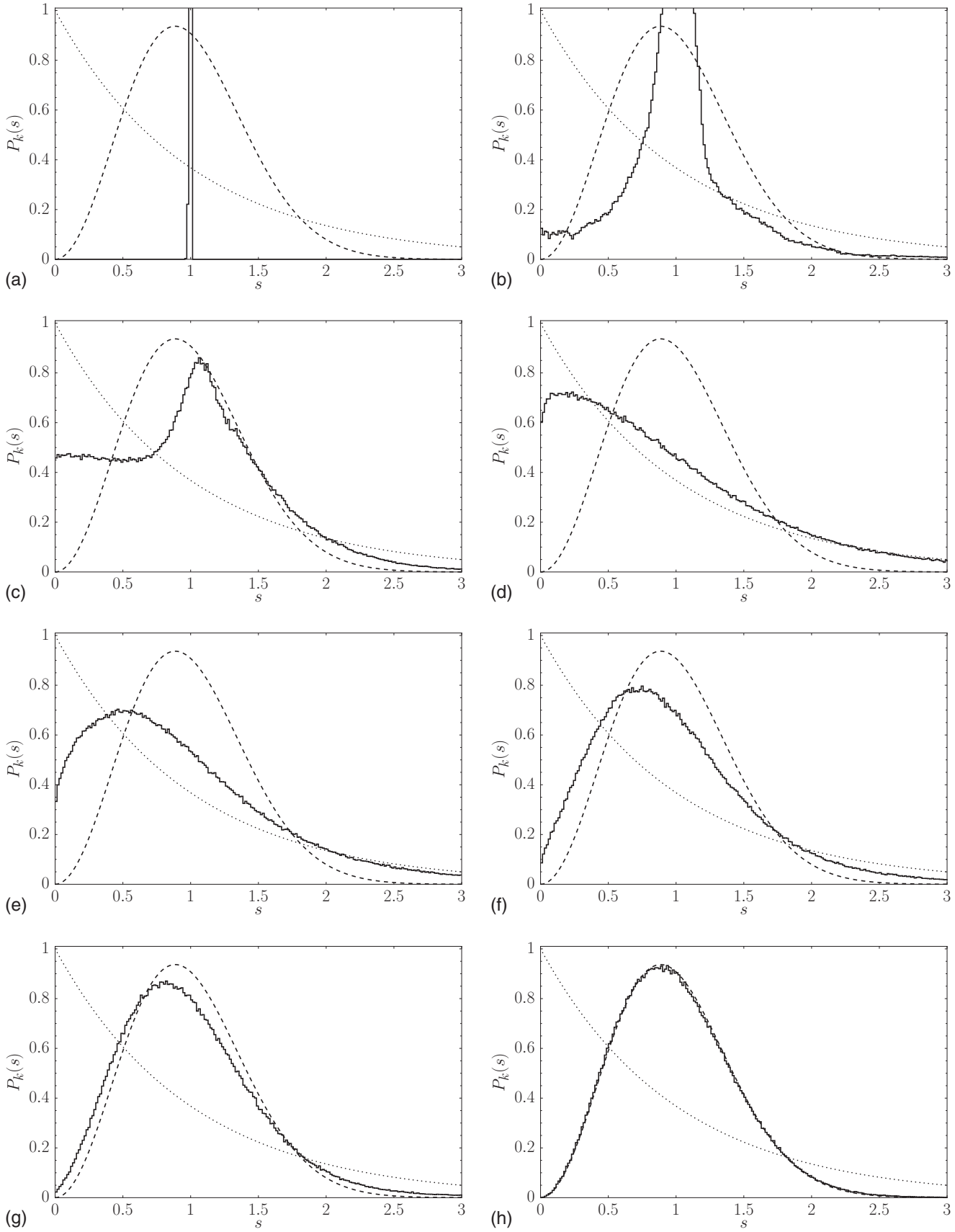

FIG. 2. Same as Fig. 1 for $\beta=2$, $n=1000$, and (a) $k=1$, (b) $k=2$, (c) $k=10$, (d) $k=200$, (e) $k=500$, (f) $k=700$, (g) $k=800$, and (h) $k=940$. Notice that the strong peak observed in Fig. 1 at $s=0$ for $\beta=1$ is absent in this case, indicating that its origin is due to time-reversal symmetry. Yet, certain degree of level clustering is still observed on a wide interval of k.

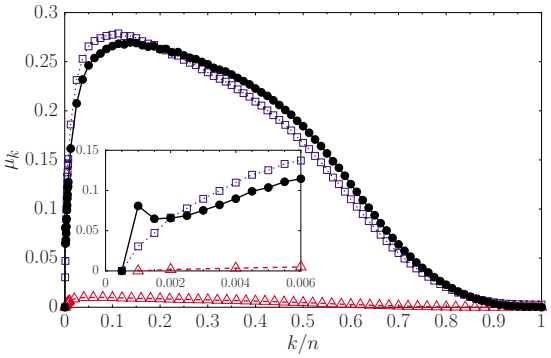

FIG. 3. (Color online) Relative measure μ_k of the number of levels contained within the first four bins of the nearest-neighbor spacing distributions as a function of k/n. The blue curve (dotted curve with squares) corresponds to the time-reversal invariant case ($\beta=1$) and the red curve (dashed curve with triangles) corresponds to the broken time-reversal case ($\beta=2$). The continuous black curve (full circles) represents the average number of Shnirelman doublets ($\beta=1$) obtained using the symmetry properties of the eigenfunctions. Inset shows details for small values of k.

$$\mathcal{H}_{0k}^{(\beta)} = \sum_{s=0}^{k} \frac{v_{s,s}^{(\beta)}}{(\mathcal{N}_s^{(k)})^2} \mathcal{P}_s\left(I_1 - \frac{1}{2}, s\right) \mathcal{P}_{k-s}\left(I_2 - \frac{1}{2}, k-s\right), \quad (4)$$

$$\mathcal{V}_k^{(\beta)} = \sum_{s>t} \frac{v_{s,t}^{(\beta)} (I_1 I_2)^{(s-t)/2}}{2\mathcal{N}_r^{(k)} \mathcal{N}_s^{(k)}} \cos[(s-t)(\phi_2 - \phi_1)] \left[\mathcal{P}_t\left(I_1 - \frac{1}{2}, s\right) + \mathcal{P}_t\left(I_1 - \frac{1}{2}, t\right) \right] \left[\mathcal{P}_{k-s}\left(I_2 - \frac{1}{2}, k-s\right) + \mathcal{P}_{k-s}\left(I_2 - \frac{1}{2}, k-t\right) \right]. \quad (5)$$

In Eqs. (4) and (5), $\mathcal{P}_t(I,s)$ are polynomials of degree t on the variable I defined as

$$\mathcal{P}_t(I,s) = \prod_{i=1}^{t} [I - (s-i)], \quad (6)$$

with s a numerical coefficient satisfying $s \geq t \geq 0$. We notice that the time-reversal symmetry properties of the ensemble are reflected in the matrix elements $v_{s,t}^{(\beta)}$.

The classical Hamiltonian $\mathcal{H}_k^{(\beta)}$ is therefore a general polynomial of degree k on the product of the actions with random coefficients, modulated by cosine functions whose argument is $\phi_2 - \phi_1$. For $\beta=1$, the matrix elements $v_{s,t}^{(\beta=1)}$ are real random numbers. Hence, time-reversal symmetry is manifested through the symmetry under reflection of both angles, i.e., $\phi_r \to -\phi_r$ for both $r=1,2$. In the case $\beta=2$, the matrix $v^{(\beta=2)}$ is complex Hermitian and the matrix elements can be written as $v_{s,t}^{(\beta=2)} = |v_{s,t}^{(\beta=1)}| \exp[i\nu_{r,s}]$, with the random phases satisfying $\nu_{r,s} = -\nu_{s,r}$ for Hermiticity. Therefore, the phases $\nu_{r,s}$ for $\beta=2$ can be included into the cosine functions, manifestly breaking the invariance under simultaneous reflections.

From Eqs. (4) and (5), the angle variables appear in the Hamiltonian $\mathcal{H}_k^{(\beta)}$ only through the combination $\phi_2 - \phi_1$. In terms of the phase-space geometry, this specific dependence corresponds to one single resonance, which implies the integrability of the classical Hamiltonian $\mathcal{H}_k^{(\beta)}$. More explicitly, we perform a canonical transformation to new action and angle variables using the generating function $W = K\phi_1 + J(\phi_2 - \phi_1)$ and obtain $I_1 = K - J$, $I_2 = J$, $\chi = \phi_1$, and $\psi = \phi_2 - \phi_1$. Substituting these expressions in Eqs. (4) and (5), the transformed Hamiltonian depends only on the angle ψ. Since the angle χ does not appear in the transformed Hamiltonian, its canonically conjugated action K is a conserved quantity, $K = I_1 + I_2 = n+1$, with n the number of bosons. Therefore, besides the conservation of the energy (the Hamiltonian is time independent), we have a second constant of motion, K. It is easy to show that the Poisson bracket between K and $\mathcal{H}_k^{(\beta)}$ is zero, thus implying that the Hamiltonian is (Liouville) integrable. For a fixed value of K, the reduced Hamiltonian $\mathcal{H}_k^{(\beta)}(J,K,\psi)$ is a time-independent one degree of freedom system with one parameter, which is always integrable. In the language of symplectic geometry, the reduced Hamiltonian $\mathcal{H}_k^{(\beta)}(J,K,\psi)$ is identical to its normal form. In these variables, the population imbalance, which is a relevant quantity in the BECs context, is given by $z = (I_1 - I_2)/(I_1 + I_2) = 1 - 2J/K$.

We finish this discussion mentioning how to relate the action-angle variables of the reduced system (J and ψ) to the actual coordinates and momenta q_r and p_r, $r=1,2$, of the two single-particle modes. This is done by a lifting procedure [25]. Integration of the equations of motion of the reduced system yields $J(t)$ and $\psi(t)$. Undoing the canonical transformation gives all $I_r(t)$ and $\phi_r(t)$. Then we use the harmonic expressions

$$I_r^{1/2} \exp[\mp i\phi_r] = (q_r \pm ip_r)/\sqrt{2}, \quad (7)$$

which relate $I_r(t)$ and $\phi_r(t)$ to local coordinates and momenta and thus yield the usual representation of the motion of each mode.

B. Phase space structure in terms of k

The essential features of the classical dynamics can be easily visualized in Poincaré sections of the reduced Hamiltonian. Since the reduced Hamiltonian is a one degree of freedom system, this representation corresponds to the level curves $\mathcal{H}_k^{(\beta)}(J,K,\psi) = \text{const}$. Therefore, the motion of a given initial condition follows the closed curve that includes the initial conditions. The explicit appearance of the square-root factors in Eq. (5) makes the classical phase-space bounded, i.e., $J \in [0,K]$ and $\psi \in [-\pi, \pi]$, and therefore has the topology of a sphere. These properties are consistent with the interpretation of the two-mode Hamiltonian as a spin system.

The phase-space structure of the unperturbed part $\mathcal{H}_{0k}^{(\beta)}(J,K)$ is trivial since J remains constant. Therefore, in a (Mercator) representation using the ψ-J plane, the phase space appears foliated in horizontal straight lines for all k, each representing a different level curve. The perturbing term $\mathcal{V}_k^{(\beta)}(J,K,\psi)$ induces new structure due to the resonance; the argument of the cosine terms are k-dependent integer mul-

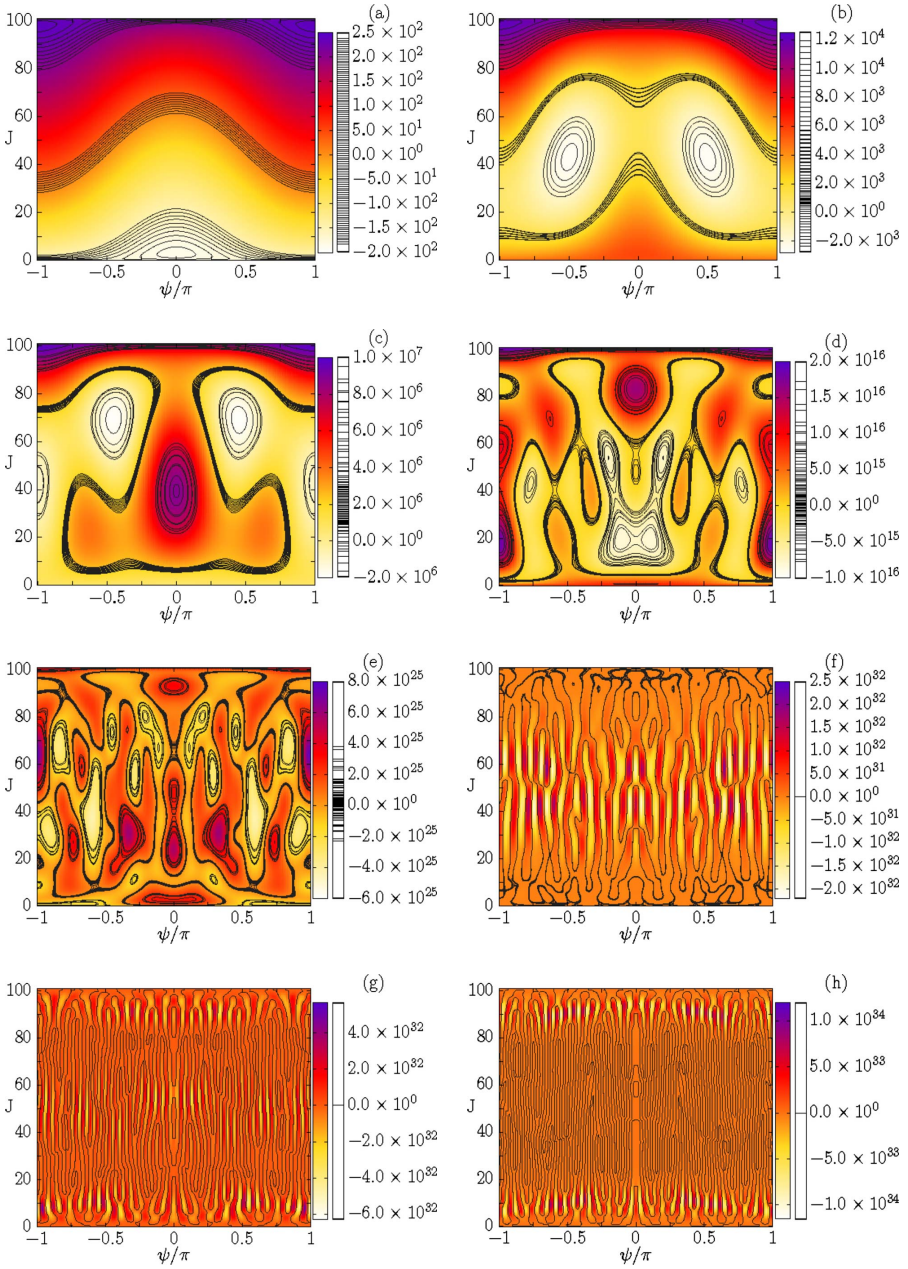

FIG. 4. (Color online) Phase space representation (level curves) of the reduced Hamiltonian $\mathcal{H}_k^{(\beta)}(J,K,\psi)$ for $\beta=1$ and $n=100$. (a) $k=1$, (b) $k=2$, (c) $k=4$, (d) $k=13$, (e) $k=29$, (f) $k=56$, (g) $k=81$, and (h) $k=100$. The continuous lines represent three groups of ten levels, taken from either edge and from the center of the spectrum. The color (gray) palette displays the overall energy scale of $\mathcal{H}_k^{(\beta=1)}(J,K,\psi)$, while the other one displays the full spectrum in the same scale. Note the clear appearance of ladders of levels associated with certain organizing centers in phase space. As k is increased, the level curves spread over all the available phase space, while the width of the spectrum decreases.

tiples of ψ. In Fig. 4, we present the phase-space structure for various values of k for $\beta=1$ and $n=100$; further details of the transition are given in the movie [23]. While the system is integrable for all k and therefore the phase space is foliated by invariant tori, the complexity of such tori increases with k. Figure 4 was constructed choosing a specific (fixed) random matrix $v^{(\beta)}$ of dimension $n+1$, which defines the case $k=n$. For $k=n-1$, we have defined the corresponding k-body interaction by using the same matrix elements $v_{r,s}^{(\beta)}$ for $r,s \leq k$, setting the remaining matrix elements to zero. This procedure can be iterated to obtain the corresponding matrix v with any desired value of k.

For $k=1$ [Fig. 4(a)], we have two harmonic-oscillator wells centered around the two stable fixed points of the system, namely, around $\psi=0$ for small values of J and $\psi=\pm\pi$ at large values of J. The invariant curves associated to initial conditions around such wells are self-retracing under time reversal, i.e., each one is mapped onto itself under the transformation $\psi\rightarrow-\psi$. At intermediate values of J, the level curves are smooth deformations of the unperturbed invariant

curves (straight lines), thus illustrating Kolmogorov-Arnold-Moser (KAM) theorem. These tori are all self-retracing under time reversal.

For $k=2$ [Fig. 4(b)], the two harmonic fixed points (at the poles of the phase-space sphere) are still observed. Yet, at intermediate values of J, we notice two other fixed points close to $\pm\pi/2$ and the associated KAM-tori surrounding them. These structures are non-self-retracing under time reversal. Consequently, those tori that satisfy the Einstein-Brillouin-Keller (EBK) quantization rule

$$S(E_i) = \frac{1}{2\pi}\oint J(E_i)d\psi = \frac{1}{2\pi}\left(\kappa_i + \frac{\alpha_i}{4}\right), \tag{8}$$

where κ_i is an integer and α_i is the associated Maslov index [27], yield two degenerate ladders of levels, each pair associated with a torus and its associated time-reversed partner; quantum effects lift the degeneracy and produce the splitting of the quasidegenerate levels. These doublets are precisely Shnirelman doublets. In Fig. 4(c), we present the case $k=4$, which displays the appearance of the new non-self-retracing wells which yield ladders of double degenerate levels. Note that there are also self-retracing tori. The ladders of levels associated with these may display accidental degeneracies with the levels of other ladders. These accidental degeneracies do not correspond to Shnirelman doublets since they may exist for the case of broken time-reversal invariance; this explains the level clustering observed for $\beta=2$ (see Fig. 3).

Increasing further the value of k increases the complexity of phase space [23]. New self-retracing and non-self-retracing wells appear in phase space, leading to Shnirelman doublets and perhaps accidental degenerate levels, respectively [see Fig. 4(d)]. Around $k\gtrsim 20$, the number of stable fixed points begins to increase more rapidly, namely, quadratically with respect to k. Increasing k seemingly leads to a clustering in the *subtropical region* around the equator ($J \approx K/2$) of the majority of the stable fixed points (see Fig. 4(f) for $k=56$). Eventually, around $k\approx 70$, the stable fixed points begin to migrate to the polar regions of the phase-space sphere, with essentially all of them in that region for $k\geq 81$ [see Figs. 4(g) and 4(h)].

As illustrated in Figs. 4, the width of the spectrum is not constant with respect to k [22]. For small k, the width is of the order of the energy scale spanned by $\mathcal{H}_k^{(\beta)}(J,K,\psi)$ [see the *spectral palette* of Figs. 4(a)–4(d)]; this allows to visually identify different regions of the phase space where the eigenvalues are located. However, for larger values of k, the width is much smaller in comparison to the full classical energy interval. In fact, for $k=n$ [Fig. 4(h)], the width is proportional to $n^{1/2}$ [1], while the full energy range is several orders of magnitude larger. Indeed, Eqs. (4) and (5) involve homogeneous polynomials of degree k on J and J spans the interval $[0,n+1]$, thus spanning a huge energy interval. In turn, violent oscillations are due to the angular dependence, which is linear on k. Note that for $k=n$ [Fig. 4(h)], the level curves associated with the energies of the spectrum spread essentially over all the phase space in such a way that it is not possible to distinguish one from another anymore, independently of their position in the spectrum.

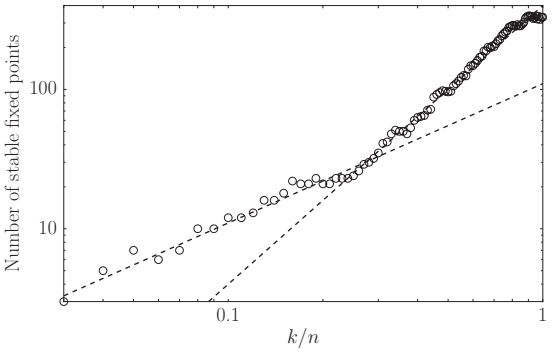

FIG. 5. Log-log plot showing the growth of the number of stable fixed points in terms of k for $n=100$. Straight lines included have slope equal to 1 or 2. Around $k\gtrsim 20$, the initial linear growth rate becomes quadratic.

The growth rate of the number of stable fixed points is illustrated in a log-log plot in Fig. 5. The plot displays an initial linear growth of the number of stable islands, which beyond $k\approx 20$ becomes quadratic in k. This figure provides a solid base for the heuristic arguments of Ref. [16]. There, it was argued that an expected quadratic growth in k of the number of stable fixed points (now shown in Fig. 5) diminishes the available phase-space area around the center of the wells. This implies that the EBK states which originally were found around those wells will now be defined on tori which are spread over more extended regions in phase space. Notice that this argument also shows that it is more difficult to have quantized states associated with non-self-retracing orbits for large values of k and thus explains that beyond certain k, the number of Shnirelman pairs diminishes fast and eventually vanishes.

V. SHNIRELMAN DOUBLETS AND THE STATISTICS OF THEIR SPLITTINGS

As shown above, for $\beta=1$, Shnirelman doublets appear and correspond to the quantization of non-self-retracing periodic orbits, i.e., orbits which are not mapped onto their selves under time-reversal invariance ($\psi\rightarrow-\psi$). Yet, these are not the only quasidegenerate levels found since there are also accidental degeneracies involving two distinct self-retracing tori that just happen to have the same energy. Note that Shnirelman doublets disappear for $\beta=2$, while the accidental degeneracies persist. Therefore, in order to distinguish the true Shnirelman doublets, we must consider the corresponding eigenfunctions, in a representation where the time-reversal invariance is appropriately manifested. For this purpose, we first analyze the structure of the eigenfunctions of the quasidegenerate states using a plane-wave decomposition which is straightforward to interpret in semiclassical terms [25]. Once we have classified the quasidegeneracies, we address the question of the statistics of the Shnirelman splittings.

A. Plane-wave decomposition of the wave functions and time-reversal symmetry

The Hamiltonian Eq. (2) is conveniently expressed in the number occupation basis or Fock basis. For a given number

of bosons n, we denote by $|n_1,n_2\rangle$ the state having n_1 bosons in the first single-particle state and n_2 bosons in the second and $n=n1+n2$. Upon diagonalization, the eigenfunctions of each realization of the ensemble are written as linear combinations of these basis states and have the form $|\Phi_r\rangle = \Sigma_{n_1+n_2=n} c^r_{n1,n2}|n_1,n_2\rangle$.

The idea now is to use a representation where the symmetry properties of the time-reversal invariance are manifested. To this end, we recall that semiclassically, the number states can be represented as plane waves on the configuration torus (defined by the angle variables), namely, $|n_i\rangle \rightarrow \exp(in_i\phi_i)|\phi_1,\phi_2\rangle$ [25]. Hence, the eigenstates can be written as $|\Phi_r\rangle = \Sigma_{n_1+n_2=n} c^r_{n1,n2} \exp[i(n_1\phi_1+n_2\phi_2)]|\phi_1,\phi_2\rangle$. Since the total boson number is conserved, the associated dimensional reduction is implemented with the same canonical transformation described for the classical action-angle variables, which is a point transformation. Then, the eigenfunction of the rth excited state is written as

$$\Phi_r(\psi) = \exp(in\chi)\sum_{n_2} c^r_{n-n_2,n2} \exp(in_2\psi). \tag{9}$$

In Eq. (9), the factor $\exp(in\chi)$ is a common phase factor for all eigenstates, which can therefore be ignored, implying that the wave functions are functions only of the angle ψ. Equation (9) defines the reduced representation of rth wave function.

As discussed above, Shnirelman doublets are related to non-self-retracing tori (under the transformation $\psi \rightarrow -\psi$) that sustain a state. The corresponding eigenfunctions $\Phi_r(\psi)$ and $\Phi_{r'}(\psi)$ appear as mixtures of wave functions localized around each symmetry-related torus. Therefore, we consider the linear combinations

$$\Phi^+_{r,r'}(\psi) = \frac{1}{\sqrt{2}}\mathrm{Re}[\Phi_r(\psi) + i\Phi_{r'}(\psi)], \tag{10}$$

$$\Phi^-_{r,r'}(\psi) = \frac{1}{\sqrt{2}}\mathrm{Re}[\Phi_r(\psi) - i\Phi_{r'}(\psi)]. \tag{11}$$

In order to identify Shnirelman doublets, we proceed as follows. First, we identify energy levels which lie very close together, which in practical terms means within the first few bins of the nearest-neighbor distribution measured in units of the mean-level spacing. One would naively think that Shnirelman doublets appear as consecutive levels; yet, accidental degeneracies due to other tori may have energies in between those of the doublets. This happens rather frequently for $k/n \gtrsim 0.2$, where the number of stable fixed points grows quadratically on k. Therefore, we must check not only degeneracy with respect to the nearest level, but within a wider range. Then, for each candidate r of a Shnirelman doublet, we consider a second level r' and construct the linear combinations given by Eqs. (10) and (11). If and only if the functions $\Phi^+_{r,r'}(\psi)$ and $\Phi^-_{r,r'}(\psi)$ are concentrated on one side of the ψ axis (either positive or negative) and among them they are in opposite sides, then we say that the levels correspond to a Shnirelman doublet. In this case, the functions

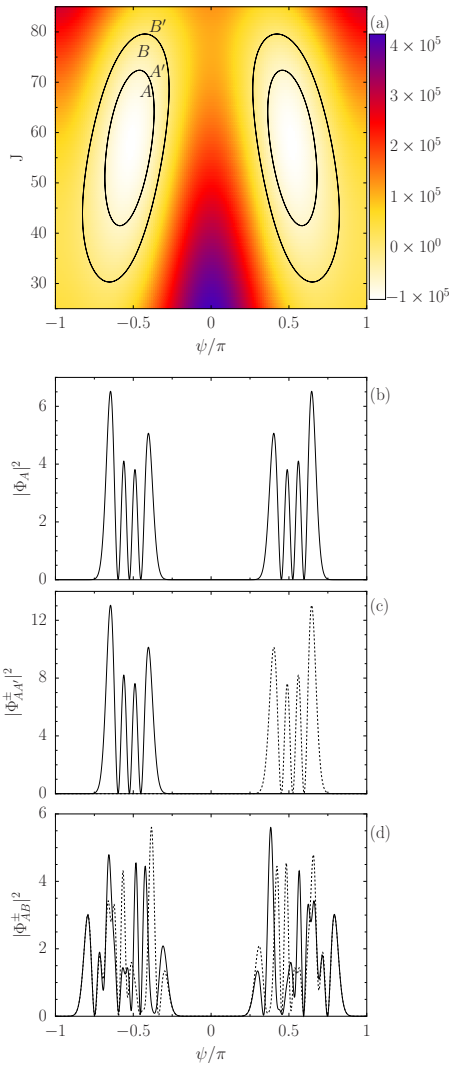

FIG. 6. (Color online) (a) Classical phase-space representation for $k=3$ showing two pairs of non-self-retracing tori. The labels indicate the symmetry-related eigenfunctions. The color (gray) code is related to the full classical energy-scale of this case. (b) Reduced representation of the square modulus of the eigenfunction A. (c) Linear combinations (10) and (11) with respect to levels A and A'; the figure shows that the linear combinations lie on opposite sides of the ψ axis and therefore the eigenfunctions are a Shnirelman doublet. (d) Result of the linear combinations when considering two non-symmetry-related nearby levels A and B.

$\Phi^+_{r,r'}(\psi)$ and $\Phi^-_{r,r'}(\psi)$ are said to be related by the time-reversal transformation $\psi \rightarrow -\psi$.

This method is illustrated in Fig. 6. In Fig. 6(a), we plot the classical phase-space representation of the non-self-retracing tori corresponding to two pairs of Shnirelman doublets belonging to the same ladder. Figures 6(b)–6(d) display the reduced representation of the modulus square of some linear combinations involving these states. Figure 6(b) displays one of the states corresponding to the tori A. In Fig. 6(c), we present the linear combinations (10)and (11) involving the states A and A'; the resulting states are localized on either side of the $\psi=0$ line, from where it is clear that these states are related by time-reversal invariance. Finally, in Fig.

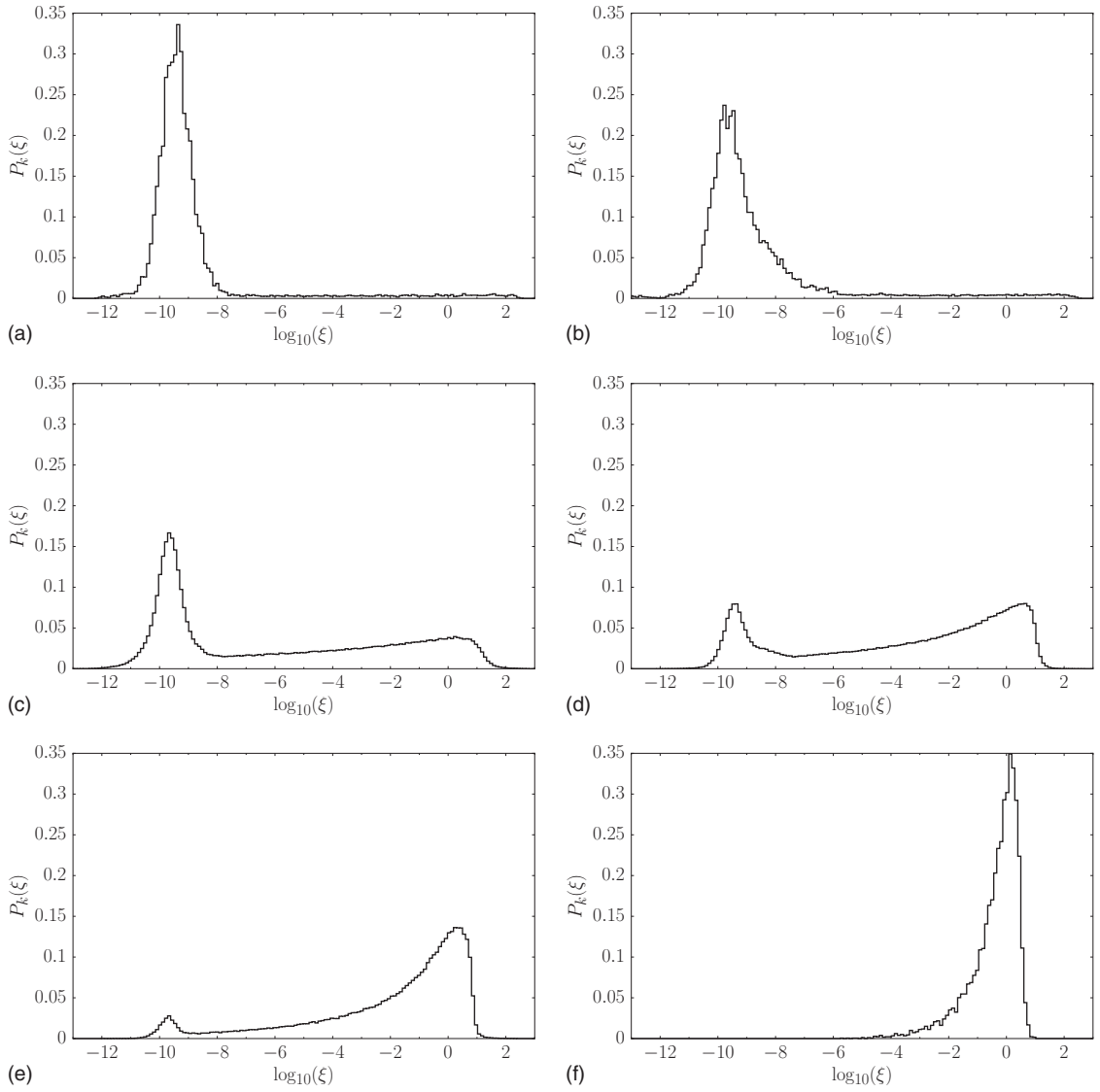

FIG. 7. Distribution $P_k(\xi)$ of the normalized spacings of the Shnirelman doublets for (a) $k=2$, (b) $k=3$, (c) $k=250$, (d) $k=750$, (e) $k=1200$, and (f) $k=1800$.

4(d), we display the linear combinations involving two states A and B which belong to the same ladder but are not related by time-reversal invariance.

B. Statistical properties of Shnirelman splittings

We are interested in the spectral statistics of the spacings of the energies E_j and $E_{j'}$ of Shnirelman doublets, i.e., the Shnirelman splittings, each one defines a characteristic tunneling time given by $T \approx \hbar/\Delta E_j$. Let E_j and $E_{j'}$ be the energies of a Shnirelman doublet of a specific realization obtained by diagonalization. We define

$$\xi'_j = 2\frac{|E_j - E_{j'}|}{|E_j + E_{j'}|}, \tag{12}$$

$$\xi_j = \frac{\xi'_j}{\bar{\xi}'}, \tag{13}$$

where $\bar{\xi}'$ is the mean value of ξ'_j taken over the corresponding realization. Therefore, the quantity ξ is a measure of the splitting E_j and $E_{j'}$ in units of the energy of the doublet, averaged over the splittings of the corresponding realization of the ensemble. The average is performed in order to compare the splittings of different realizations of the ensemble; hence, $\bar{\xi}=1$. Then, ξ is a kind of unfolded spacings of the Shnirelman doublets.

In Fig. 7, we present the distribution of the spacings of Shnirelman doublets $P_k(\xi)$ for various values of k. These results were obtained for $n=2000$ and 1000 realizations of the ensemble. For $k=2$, this distribution displays a large narrow peak close to $\xi=1.3\times10^{-9}$ which is not symmetric. The peak decays very fast, acquiring a somewhat constant tail

toward larger values of ξ; this tail vanishes after $\xi=100$. That is, while most doublets have a very small spacing in the normalized units used here, the doublets close to the edge of the ladder have larger spacings. For $k=3$, similar results hold; yet, it is worth noticing that the distribution becomes somewhat wider with respect to the result for $k=2$. As k increases further, the behavior of $P_k(\xi)$ becomes more complex, with a gradual appearance of a second peak [close to $\xi=1$ in Fig. 7(c)]. For a larger value of k around $k\approx 750$ [see Fig. 7(d)], both peaks have a similar amplitude; beyond this value of k, the left peak diminishes smoothly, eventually vanishing, yielding again a single peak distribution, this time for values centered around $\xi\approx 1$.

The transition in $P_k(\xi)$ described above can be understood as follows. For small values or moderate values of k, the unimodal distribution reflects the existence of one or more ladders of Shnirelman doublets. Each ladder has a number of doublets, the spacing with in each doublet becoming larger (smaller tunneling times) as we climb up the ladder. Imposing $\bar{\xi}=1$ yields the long tail observed in the distribution. By increasing the value of k, the distribution $P_k(\xi)$ becomes bimodal, displaying a second peak centered around $\xi=1$. That is, the doublets have either a very small splitting or splittings of order 1. As mentioned above, larger splittings are attributed to the last doublets of a ladder around a stable fixed point. In order to have a significant number of them without increasing the number of small splittings, we conclude that their ladder must consist of very few (one or two) Shnirelman doublets. This idea is consistent with the fact that, for large value of k, only a single doublet is observed around the stable fixed points where the quantization condition Eq. (8) holds. Note that the latter case implies again a unimodal distribution $P_k(\xi)$, this time the peak being centered around 1, as it is observed numerically.

VI. SUMMARY AND CONCLUSIONS

In this paper, we have investigated the nearest-neighbor spacing distribution of the k-body embedded ensembles for bosons distributed in two levels for $\beta=1$ and $\beta=2$. For $\beta=1$, we found a large peak at $s=0$ in a large interval of k which indicates the presence of degeneracies. This peak is quite robust in terms of k, disappearing only when k is very close to n, the total number of bosons. For $\beta=2$, the peak is absent, despite of the fact that there are accidental quasidegeneracies which yield small spacings; hence, the large peak is a consequence of the time-reversal invariance of the ensemble. We showed that this peak is associated with Shnirelman doublets, which semiclassically correspond to the quantization of tori that are non-self-retracing under time reversal. These results provide further evidence on the integrability of the ensemble [15] based now on the spectral properties of the ensemble and therefore explain the nonergodic properties of the ensemble [22]. The fact that Shnirelman doublets are not observed for k very close to n, where GOE spectral statistics hold, is due to the fact that the non-self-retracing tori which would yield such doublets have a extremely small action, as shown in the phase-space representation of this case.

We also found for $\beta=1$ that the number of Shnirelman quasidegeneracies displays a dependence upon k (cf. Fig. 3). Moreover, the statistics of the normalized splittings do display also a dependence on k; in particular, for $k=2$ and $k=3$ which are the physically relevant cases, we observe certain qualitative differences. We believe that these results may be interesting for understanding and modeling three-body interactions in Bose-Einstein condensates.

Indeed, the existence of Shnirelman doublets opens the possibility of producing or observing other type of Josephson-like oscillations in two-mode Bose-Einstein condensates which may not be centered around zero population imbalance [see, e.g., Figs. 4(a) and 4(b)]. To clarify this, we must emphasize that the degenerate states present in two-mode Bose-Einstein condensates [14] are not Shnirelman doublets; the degeneracies are due to the fact that the potential wells are indistinguishable, i.e., they are associated with the quantization of two tori related by the symmetry $J\rightarrow n+1-J$. Therefore, in order to produce Shnirelman doublets, we must have the possibility of tuning *all* two-body interaction matrix elements at will, which may require considering also two species condensates. Once this is done, the statistical properties of Shnirelman doublets could be used to characterize the role of interactions beyond $k=2$. This will be the subject of a future work.

ACKNOWLEDGMENTS

We have profited from discussions and suggestions with F. Leyvraz, C. Jung, and T. H. Seligman. We acknowledge financial support from Projects No. IN-107308 (DGAPA-UNAM) and No. 57334-F (CONACyT). S.H.Q. was supported by CONACyT.

[1] T. Guhr, A. Mueller-Gröling, and H. A. Weidenmüller, Phys. Rep. **299**, 189 (1998).
[2] K. K. Mon and J. B. French, Ann. Phys. (N.Y.) **95**, 90 (1975).
[3] L. Benet and H. A. Weidenmüller, J. Phys. A **36**, 3569 (2003).
[4] O. Morsch and M. Oberthaler, Rev. Mod. Phys. **78**, 179 (2006).
[5] R. Gati and M. K. Oberthaler, J. Phys. B **40**, R61 (2007).
[6] M. R. Andrews *et al.*, Science **275**, 637 (1997).
[7] G. J. Milburn, J. Corney, E. M. Wright, and D. F. Walls, Phys. Rev. A **55**, 4318 (1997).
[8] M. Albiez, R. Gati, J. Folling, S. Hunsmann, M. Cristiani, and M. K. Oberthaler, Phys. Rev. Lett. **95**, 010402 (2005).
[9] F. Cataliotti *et al.*, Science **293**, 843 (2001); B. P. Anderson and M. A. Kasevich, *ibid.* **282**, 1686 (1998).
[10] A. Micheli, D. Jaksch, J. I. Cirac, and P. Zoller, Phys. Rev. A **67**, 013607 (2003).

[11] R. Franzosi and V. Penna, Phys. Rev. A **65**, 013601 (2001).
[12] W. Zwerger, J. Opt. B: Quantum Semiclassical Opt. **5**, S9 (2003).
[13] I. Bloch, J. Phys. B **38**, S629 (2005); D. Jaksch and P. Zoller, Ann. Phys. (N.Y.) **315**, 52 (2005).
[14] A. N. Salgueiro *et al.*, Eur. Phys. J. **D44**, 537 (2007).
[15] L. Benet, C. Jung, and F. Leyvraz, J. Phys. A **36**, L217 (2003).
[16] L. Benet, F. Leyvraz and T. H. Seligman, Phys. Rev. E **68**, 045201(R) (2003).
[17] M. V. Berry and M. Tabor, Proc. R. Soc. London, Ser. A **356**, 375 (1977).
[18] S. W. McDonald and A. N. Kaufman, Phys. Rev. Lett. **42**, 1189 (1979); G. Casati, F. Valz-Gris, and I. Guarneri, Lett. Nuovo Cimento **28**, 279 (1980); M. V. Berry, Ann. Phys. (N.Y.) **131**, 163 (1981); *The Wave-Particle Dualism*, edited by S. Diner *et al.* (D. Reidel, Dordrecht, 1984), p. 231; O. Bohigas, M.-J. Giannoni, and C. Schmit, Phys. Rev. Lett. **52**, 1 (1984).
[19] A. I. Shnirelman, Usp. Mat. Nauk **30**, 265 (1975); A. I. Shnirelman, *KAM Theory and Semiclassical Approximations to Eigenfunctions* (Springer, Berlin, 1993).
[20] B. V. Chirikov and D. L. Shepelyansky, Phys. Rev. Lett. **74**, 518 (1995); B. V. Chirikov, Budker INP Report No. 96-57, 1996 (unpublished).
[21] H. P. Büchler, A. Micheli, and P. Zoller, Nat. Phys. **3**, 726 (2007); P. R. Johnson, E. Tiesinga, J. V. Porto, and C. J. Williams, New J. Phys. **11**, 093022 (2009), and references therein.
[22] T. Asaga *et al.*, Europhys. Lett. **56**, 340 (2001); T. Asaga *et al.*, Ann. Phys. (N.Y.) **298**, 229 (2002).
[23] See supplementary material at http://link.aps.org/supplemental/10.1103/PhysRevE.81.036218 Movie1 shows a movie of the nearest-neighbor distribution $P_k(s)$ for $\beta=1$; each frame corresponds to a different value of k, as indicated. Movie2 is the corresponding movie for the case $\beta=2$. Movie3 is a movie on the phase-space representation of the reduced Hamiltonian for $n=100$ and $\beta=1$. The level curves represent the energy eigenvalues of the corresponding quantized Hamiltonian.
[24] J. Marklof, *Proceedings of the 3rd European Congress of Mathematics, Barcelona, 2000*, Progress in Mathematics (Birkhuser, Basel, 2001), Vol. 202, p. 421.
[25] M. P. Jacobson *et al.*, J. Chem. Phys. **111**, 600 (1999); C. Jung, H. S. Taylor, and E. Atilgan, J. Phys. Chem. A **106**, 3092 (2002); H. Waalkens, C. Jung, and H. S. Taylor, *ibid.* **106**, 911 (2002); C. Jung, C. Mejía-Monasterio, and H. S. Taylor, J. Chem. Phys. **120**, 4194 (2004).
[26] W. Heisenberg, Z. Phys. **33**, 879 (1925).
[27] R. G. Littlejohn and J. M. Robbins, Phys. Rev. A **36**, 2953 (1987).